

Lawrence Berkeley National Laboratory

Lawrence Berkeley National Laboratory

Title

Ultrafast Mid-Infrared Intra-Excitonic Response of Individualized Single-Walled Carbon Nanotubes

Permalink

<https://escholarship.org/uc/item/04s2k6rt>

Author

Wang, Jigang

Publication Date

2011-01-06

Peer reviewed

Ultrafast Spectroscopy of Mid-Infrared Internal Exciton Transitions of Separated Single-Walled Carbon Nanotubes

Jigang Wang,^{1,2} Matt W. Graham,³ Yingzhong
Ma,^{3,4} Graham R. Fleming,³ and Robert A. Kaindl¹

¹*Materials Sciences Division, E.O. Lawrence Berkeley
National Laboratory, Berkeley, California 94720, USA*

²*Department of Physics and Astronomy and Ames Laboratory,
Iowa State University, Ames, Iowa 50010, USA*

³*Department of Chemistry, University of California
at Berkeley and Physical Biosciences Division,*

E. O. Lawrence Berkeley National Laboratory, Berkeley, California 94720, USA

⁴*Chemical Sciences Division, Oak Ridge National Laboratory, Oak Ridge, TN 37831, USA*

Abstract

We report a femtosecond mid-infrared study of the broadband low-energy response of individually separated (6,5) and (7,5) single-walled carbon nanotubes. Strong photoinduced absorption is observed around 200 meV, whose transition energy, oscillator strength, resonant chirality enhancement and dynamics manifest the observation of quasi-1D intra-excitonic transitions. A model of the nanotube $1s$ - $2p$ cross section agrees well with the signal amplitudes. Our study further reveals saturation of the photoinduced absorption with increasing phase-space filling of the correlated e - h pairs.

PACS numbers: 78.47.-p, 78.47.J-, 78.30.Na, 78.67.Ch, 73.22.-f

The quasi-1D confinement of photoexcited charges in single-walled carbon nanotubes (SWNTs) gives rise to strongly enhanced Coulomb interactions and large exciton binding energies on the 100 meV energy scale. These amplified electron-hole ($e-h$) correlations are a key aspect of nanotube physics [1]. With the availability of individually separated SWNT ensembles, this strong excitonic behavior was confirmed by interband absorption-luminescence maps [2], two-photon excited luminescence [3, 4], and ultrafast spectroscopy [5]. Optical interband probes, however, are limited by symmetry and momentum to detect only a small subset of excitons.

As illustrated in Fig. 1(a) in a two-particle scheme, SWNT excitons are characterized by a center-of-mass momentum K and by an internal quantum state (designated here as $1s$, $2s$, $2p$, ...) that accounts for the relative charge motion. Each state splits into even (g) and odd (u) parity levels corresponding to different superpositions of the cell-periodic wavefunctions of the underlying graphene lattice [4]. This entails a series of optically "dark" excitons, including the $1s$ -(g) lowest-energy exciton that lacks coupling in both single- and two-photon interband spectroscopy [3, 4]. Splitting into singlet and triplet spin states additionally restricts interband optical coupling [6]. Finally, interband transitions are limited to excitons around $K \approx 0$ due to momentum conservation.

Intra-excitonic transitions between low-energy levels of excitons with the same cell-periodic symmetry [arrows, Fig. 1(a)] represent a fundamentally different tool, analogous to atomic absorption spectroscopy. In contrast to interband absorption that measures the ability to *generate* $e-h$ pairs, intra-excitonic absorption detects existing excitons via transitions from the $1s$ ground state to higher relative-momentum states [7, 8]. Being independent of K ,

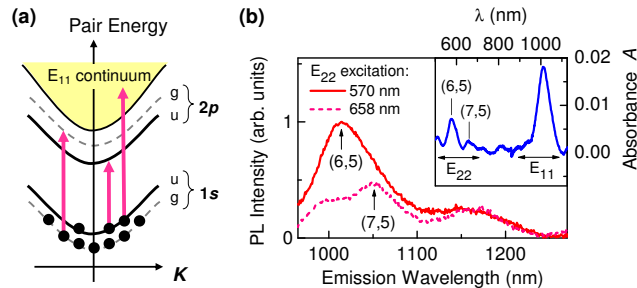


FIG. 1: (Color online) (a) Two-particle $e-h$ pair dispersion, illustrating exciton bands and $1s \rightarrow 2p$ intra-excitonic transitions (arrows). (b) PL spectra of the sample under resonant E_{22} excitation. Inset: Near-IR absorbance after subtracting background scattering.

it is sensitive to genuine exciton populations across momentum space. As the cell-periodic component of the wavefunction remains unchanged, intra-excitonic absorption is also unrestricted by the exciton ground state symmetry [7]. Applied to individualized SWNTs, intra-excitonic resonances can thus measure both bright and dark excitons and should occur in the mid-infrared (mid-IR) after ultrafast excitation. In contrast to extensive interband nanotube studies [9–12], only a few ultrafast intra-band experiments have been carried out which focus largely on nanotube bundles [13–16]. THz experiments on photoexcited bundled tubes revealed a non-Drude response attributed to small-gap metallic tubes or inter-tube charge separation [13, 14]. Mid-IR transient absorption was also observed in bundled nanotubes and assigned to transitions from allowed to dipole-forbidden excitons [15, 16].

In this Letter, we report ultrafast optical-pump, mid-IR-probe studies of individually separated (6,5) and (7,5) SWNTs. Transient spectra after photoexcitation evidence strong mid-IR absorption around 200 meV, in accordance with intra-excitonic transitions of strongly-bound e - h pairs in semiconducting nanotubes. The absorption cross section of $4 \cdot 10^{-15} \text{ cm}^2$ agrees closely with calculations of quasi-1D intra-excitonic $1s$ - $2p$ dipole transitions presented here. The excitation-wavelength dependence and kinetics further underscore the excitonic origin of the mid-IR response, and its intensity dependence scales quantitatively with a model of phase-space filling expected for quasi-1D excitons. This intra-excitonic absorption represents a sensitive tool to probe correlated e - h pairs in SWNTs, unhindered by interband dipole or momentum restrictions.

Ultrafast spectroscopy was carried out in transmission using widely tunable femtosecond (fs) pulses in the mid-IR and visible range. Two near-IR optical parametric amplifiers (OPAs) were pumped by a 1-kHz, 28-fs Ti:sapphire amplifier. Resonant and off-resonant interband excitation was achieved using the frequency-doubled OPA or a fraction of the fundamental. The output of the second OPA was difference-frequency mixed in GaSe to generate ≈ 100 fs mid-IR probe pulses tunable from 4-12 μm [17]. We study individually separated Co-Mo-catalyst grown SWNTs of mainly (6,5) and (7,5) chiralities [18] embedded in 50- μm thick polyethylene (PE). Importantly, PE ensures transparency throughout our mid-IR probe range, except for a narrow CH-bend vibration at 178 meV. The films were fabricated by drying PE solutions in decalin mixed with micelle-dispersed SWNTs, after transferring SWNTs suspended in H_2O with NaDDBS to the PE solution via ultrasound and thermal treatments. In Fig. 1(b), the sample’s photoluminescence (PL) spectra for

resonant (6,5) and (7,5) E_{22} excitation clearly exhibit the distinct E_{11} emission of these individualized SWNT chiralities, with only weak emission from bundled tubes around 1160 nm [19]. The absorption spectrum [inset, Fig. 1(b)] also exhibits the distinct E_{11} and E_{22} absorption peaks.

Ultrafast spectrally-resolved mid-IR transmission changes $\Delta T/T$ are shown in Fig. 2 for different time delays Δt after 800 nm photoexcitation at room temperature. A strong photo-induced absorption appears within the time resolution after photoexcitation [Fig. 2(b), $\Delta t = 200$ fs] and decays on a ps timescale [Fig. 2(c)-(d)]. The transient spectra are characterized by a broadly sloping, asymmetric resonance around 200 meV, with a step-like onset above 160 meV. This mid-IR resonance occurs in the transparent region far below the lowest interband exciton ($E_{11} \simeq 1.2$ eV) and intersubband transitions ($E_{22} - E_{11} \geq 0.6$ eV). The peak energy is close to the (6,5) and (7,5) $1s$ - $2p$ energy splitting in two-photon luminescence studies and calculations [3, 4, 20]. Thus, we associate this absorption with intra-excitonic transitions between $1s$ and $2p$ exciton levels of opposite parity. Both dipole-allowed and optically-dark $1s$ excitons can fundamentally contribute to this response. The dynamics exhibits a pulse-width limited rise of the photoinduced mid-IR absorption (inset, Fig. 2), which indicates rapid exciton formation.

We should comment on the asymmetric line shape observed in Fig. 2. The observed rapid onset and asymmetry point to a predominantly inhomogeneous broadening, resulting

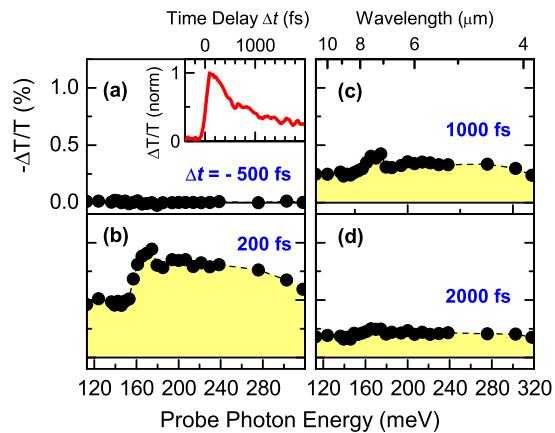


FIG. 2: (Color online) (a)-(d) Ultrafast spectrally-resolved mid-IR transmission changes after 800 nm excitation for four different delays Δt as indicated. Inset: normalized dynamics of the mid-IR transmission probed at $4.4 \mu\text{m}$ wavelength.

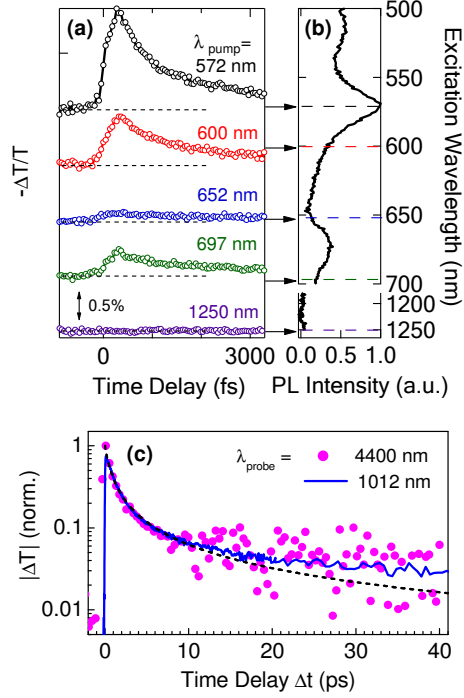


FIG. 3: (Color online) (a) Pump wavelength dependence on and off-resonant to the (6,5) and (7,5) E_{22} transitions. Traces are offset for clarity, and measured at $4.4 \mu\text{m}$ with $260 \mu\text{J}/\text{cm}^2$ excitation fluence. (b) PL-excitation spectrum for fixed E_{11} emission at 1012 nm. (c) Normalized mid-IR dynamics (dots) after 572 nm excitation. Thick line: E_{11} transmission change, scaled to the mid-IR signal at long delays. Dashed line: bimolecular decay $|\Delta T| \propto (1 + \gamma t)^{-1}$ with $\gamma = 1.5 \text{ ps}^{-1}$.

in a large $\simeq 100 \text{ meV}$ line width composed of multiple transitions, which matches well with similar spectral features in two-photon PL experiments [3, 4]. We attribute the higher-energy tail to intra-excitonic transitions from the $1s$ into higher-lying np bound states and into the broad continuum of unbound pairs, consistent with the asymmetric intra-excitonic spectra of quasi-2D e - h pairs [8]. Note that a much narrower peak seems to exist around 170 meV which we assign as an artifact [21]. Low-energy absorption is also observed below 160 meV which can arise e.g. from fluctuations of the dielectric environment around the nanotube and other chiral tube species [22].

To further substantiate the nature of the response, Fig. 3(a) shows the excitation wavelength dependence. Resonant photoexcitation of the (6,5) and (7,5) interband E_{22} transitions, at 572 nm and 697 nm respectively, leads to significant enhancement of the transient mid-IR absorption. The amplitude closely tracks the PL-excitation spectrum [Fig. 3(b)],

which clearly underscores the tube-specific origin of the transient mid-IR response. This conclusion is further supported by the disappearance of the photoinduced signal for excitation below the E_{11} transition [1250 nm, Fig. 3(a)]. Hence, the observed photo-induced absorption arises from intra-excitonic transitions of (6,5) and (7,5) SWNTs. The mid-IR dynamics after (6,5) E_{22} excitation is shown in Fig. 3(c) on an extended timescale, revealing a strongly non-exponential decay [dots, Fig. 3(c)] over several 10 ps. The dynamics closely follows the E_{11} exciton bleaching [solid line, Fig. 3(c)], confirming that the mid-IR signals originate from excitations in the E_{11} manifold. Thermal broadening $k_B T \simeq 26$ meV at 300 K entails comparable occupation of dark and bright excitons (split by $\simeq 10$ meV), which enables this comparison. The decay has a bimolecular shape [dashed line, Fig 3(c)], similar to the fs kinetics of excitons in individualized SWNT suspensions explained by exciton-exciton annihilation [9], which further underscores the excitonic origin of the mid-IR response.

The mid-IR transmission changes can be used to estimate the absorption cross section σ_{MIR}^{\parallel} of the intra-excitonic transition, whose dipole is oriented parallel to the SWNT axis. It is defined as $\sigma_{MIR}^{\parallel} = 3 \ln(1 - \Delta T/T) / n_{exc}$, where ΔT is the initial transmission change and n_{exc} the photoexcited density. The factor 3 accounts for the random SWNT orientation. Considering (6,5) E_{22} resonant excitation in Fig. 3(a) one has $\Delta T/T \approx 1.7\%$ and $n_{exc} = (F/\hbar\omega) \times \ln(10)A = 1.2 \times 10^{13} \text{ cm}^{-2}$, given $F = 260 \mu\text{J}/\text{cm}^2$ and $A \simeq 0.007$ [inset, Fig. 1(b)]. This yields the experimentally-derived value for the cross section of $\sigma_{MIR}^{\parallel} \simeq 4 \times 10^{-15} \text{ cm}^2$.

For comparison, we calculate the intra-excitonic $1s$ - $2p$ cross section based on a model of Wannier-like excitons in SWNTs. The normalized $1s$ and $2p$ wavefunctions of Coulomb-bound e - h pairs on a cylindrical surface are [23]

$$\begin{aligned} \psi_{1s}(x) &= \sqrt{\frac{8}{(a_B^*)^3 \alpha_{1s}^3 B_{1s}}} |x| e^{-\frac{|x|}{a_B^* \alpha_{1s}}} U(1 - \alpha_{1s}, 2, \frac{2|x|}{a_B^* \alpha_{1s}}), \\ \psi_{2p}(x) &= \sqrt{\frac{2}{(a_B^*)^3}} x e^{-\frac{|x|}{a_B^*}}, \end{aligned} \quad (1)$$

where x measures the distance along the nanotube axis and $a_B^* = 4\pi\epsilon\epsilon_0\hbar^2/\mu e^2$ is the effective 3D Bohr radius with reduced mass μ and permittivity ϵ . Furthermore, U is Kummer's confluent hypergeometric function of the second kind and $B_{1s} \equiv 2 \int_0^\infty y^2 e^{-y} [U(1 - \alpha_{1s}, 2, y)]^2 dy$ is a normalization constant. The binding energies are $E_{1s} = -\text{Ry}^*/(\alpha_{1s})^2$ and $E_{2p} = -\text{Ry}^*$, where $\text{Ry}^* \equiv \hbar^2/(2\mu a_B^{*2})$ is the 3D effective Rydberg energy. Also, α_{1s} is a scaling parameter that depends on the SWNT nanotube radius r_{NT} via $\ln(\alpha_{1s}) - \Psi(1 - \alpha_{1s}) - (2\alpha_{1s})^{-1} \equiv$

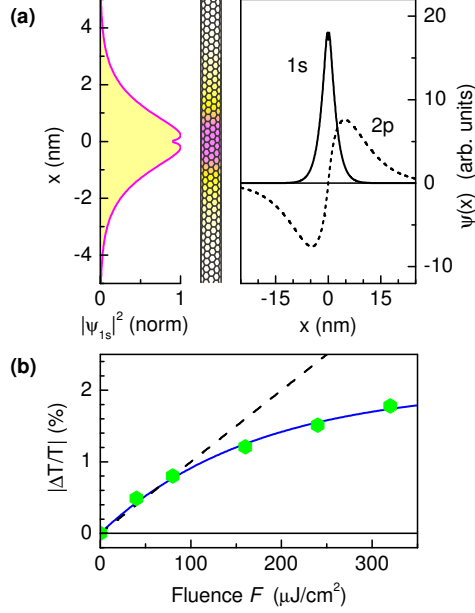


FIG. 4: (Color online) (a) Squared wavefunction amplitude $|\psi_{1s}(x)|^2$ compared to the (6,5) SWNT scale (left), and bare $1s$ and $2p$ wavefunctions (right). (b) pump fluence dependence of the initial mid-IR transmission change (dots) after resonant (6,5) E_{22} excitation. Solid line: model explained in the text, dashed line: linear scaling (guide to the eyes).

$\ln(r_{\text{NT}}) - 2\Psi(1)$ where Ψ is the digamma function [23]. For the (6,5) and (7,5) SWNTs studied here, we have $r_{\text{NT}} \simeq 0.4$ nm which entails $\alpha_{1s} = 0.33$, and $\mu \simeq 0.067$ from interpolated carrier effective masses [24]. The scale and shape of the resulting exciton wavefunctions are shown in Fig. 4(a). For this, the permittivity which depends on the local dielectric environment was adjusted to $\epsilon = 6$ to reproduce the intra-excitonic splitting $E_{2p} - E_{1s} \simeq 0.2$ eV from the experiment, which corresponds to a binding energy of 233 meV.

With the above, we obtain the $1s$ - $2p$ intra-excitonic oscillator strength of quasi-1D excitons in SWNTs

$$f_{1s \rightarrow 2p} \equiv \frac{128 \mu a_B^2 \alpha_{1s}^5}{\hbar^2 B_{1s}} (E_{2p} - E_{1s}) \times \left(\int_0^\infty s^3 e^{-s(1+\alpha_{1s})} U(1 - \alpha_{1s}, 2, 2s) ds \right)^2 \quad (2)$$

For our specific parameters, $f_{1s \rightarrow 2p} = 0.41$. Transitions into higher bound np levels ($n > 2$) were also calculated but are very weak and add less than 15% in spectral weight. The *spectrally-integrated* absorption cross section is then determined as $\sigma_{1s \rightarrow 2p}^{\text{Int}} =$

$2\pi^2 e^2 / (4\pi\epsilon_0 \mu c n) \times f_{1s \rightarrow 2p} = 4.4 \times 10^{-13} \text{ cm}^2 \text{ meV}$, where $n = 1.5$ is the polymer refractive index. Spreading this absorption across $\approx 100 \text{ meV}$ results in an estimated $1s$ - $2p$ intra-excitonic cross section of $\sigma_{1s \rightarrow 2p} \simeq 4.4 \times 10^{-15} \text{ cm}^2$, in very close agreement with our experiment. Full modeling of the asymmetric mid-IR intra-excitonic line shape in Fig. 2 is beyond the scope of the Wannier-exciton model. However, the above illustrates a general consistency between the observed mid-IR signal amplitude and the quasi-1D $1s$ - $2p$ intra-excitonic cross section, motivating more sophisticated theory to calculate bound-bound and bound-continuum spectra with chirality-specific SWNT wave functions.

The transient mid-IR absorption represents a strong oscillator comparable to the interband absorption. In the photoexcited state, this low-energy oscillator strength is derived via transfer from the interband exciton peaks, i.e. from E_{11} bleaching [10, 11]. As plotted in Fig. 4(b), with increasing excitation fluence, the mid-IR amplitude $|\Delta T/T|$ exhibits a distinctly nonlinear behavior. This finding is well described by a saturation model $\Delta T \propto 1 - e^{-F/F_s}$, shown as the solid line in Fig. 4(b) for $F_s = 170 \mu\text{J}/\text{cm}^2$. This corresponds to a 1D saturation density $n_s = \sigma_{22}^{\text{eff}} \times F_s / \hbar\omega$, where σ_{22}^{eff} is the effective E_{22} absorption cross section per unit nanotube length. The cross section of (6,5) SWNTs was recently found to be $\sigma_{22}^{\parallel} \simeq 85 \text{ nm}^2/\mu\text{m}$ for light polarized parallel to the nanotube axis, such that $\sigma_{22}^{\text{eff}} = 1/3 \times \sigma_{22}^{\parallel}$ [25]. This yields from our experiment a saturation density $n_s = 1.4 \times 10^6 \text{ cm}^{-1}$ corresponding to an average exciton spacing $d_{XX} \approx 7 \text{ nm}$. The value is close to the saturation density extrapolated from E_{11} interband bleaching at lower densities [11], while surpassing the saturation of time-averaged PL by more than an order of magnitude [12]. The difference occurs since PL depends on density-dependent decay times that saturate at lower densities, while our study detects the initial pair density. For comparison, we consider phase-space filling (PSF), i.e. the increasing occupation of the constituent Fermion states of the exciton many-particle wavefunction [26]. The PSF density is given by $N_S^{\text{PSF}} = L / [\sum_k \psi_k |\psi_k|^2 / \psi(x=0)]$, where ψ_k are the Fourier coefficients of the exciton wavefunction $\psi(x)$, and L is the normalization length [11, 26, 27]. For our quasi-1D $1s$ exciton wavefunction [Fig. 4(a)] this yields $N_S^{\text{PSF}} = 2.5 \times 10^6 \text{ cm}^{-1}$. Hence, the mid-IR response approaches yet remains somewhat below the limit imposed by phase space filling.

In conclusion, intra-excitonic transitions are both a direct consequence and a measure of e - h correlations. Our experiments provide new insights into the chirality-specific femtosecond mid-IR response of electronic excitations in individually separated SWNTs. A photo-induced

absorption around 200 meV was observed, manifesting quasi-1D intra-excitonic transitions in close agreement with the calculated $1s$ - $2p$ oscillator strength. The (6,5)/(7,5) chirality-specific enhancement and non-exponential kinetics of the transient mid-IR absorption further underscores its excitonic origin. We believe that the mid-IR probe, extended e.g. into the low-temperature or low-density limit, will provide a versatile spectroscopic tool to investigate bound quasi-1D e - h pairs and their internal electronic structure independent of interband symmetry.

This work was supported by the Office of Science, U.S. DOE via contract DE-AC02-05CH11231 with initial provision from LDRD. Manuscript finalization was also supported by Ames Laboratory, DOE contract DE-AC02-07CH11358. SWNTs were characterized at the Molecular Foundry, and prepared at U.C. Berkeley as supported by NSF. M.W.G. thanks NSERC for a graduate fellowship.

-
- [1] see e.g. M. S. Dresselhaus, G. Dresselhaus, R. Saito, and A. Jorio, *Annu. Rev. Phys. Chem.* **58**, 719 (2007).
 - [2] M. J. O'Connell *et al.*, *Science* **297**, 593 (2002).
 - [3] F. Wang, G. Dukovic, L. E. Brus, and T. F. Heinz, *Science* **308**, 838 (2005).
 - [4] J. Maultzsch *et al.*, *Phys. Rev. B* **72** 241402 (2005).
 - [5] Y.-Z. Ma *et al.*, in: *Carbon Nanotubes*, edited by A. Jorio, G. Dresselhaus, and M. S. Dresselhaus, *Topics Appl. Physics* **111**, 321 (Springer Verlag, Berlin, 2008).
 - [6] J. Jiang *et al.*, *Phys. Rev. B* **75** 035407 (2007); E. B. Barros *et al.*, *Phys. Rev. B* **73**, 241406 (2006).
 - [7] T. Ideguchi, K. Yoshioka, A. Mysyrowicz, and M. Kuwata-Gonokami, *Phys. Rev. Lett.* **100**, 233001 (2008).
 - [8] R. A. Kaindl *et al.*, *Nature* **423**, 734 (2003); R. A. Kaindl *et al.*, *Phys. Rev. B* **79**, 045320 (2009).
 - [9] Y.-Z. Ma *et al.*, *J. Chem. Phys.* **120**, 3368 (2004); Y.-Z. Ma *et al.*, *Phys. Rev. Lett.* **94**, 157402 (2005).
 - [10] F. Wang *et al.*, *Phys. Rev. B* **70**, 241403(R) (2004); G. N. Ostojic *et al.*, *Phys. Rev. Lett.* **94**, 097401 (2005); O. J. Korovyanko *et al.*, *Phys. Rev. Lett.* **92**, 017403 (2004).

- [11] L. Luer *et al.*, Nature Phys. **5**, 54 (2009).
- [12] Y. Murakami and J. Kono, Phys. Rev. Lett. **102**, 037401 (2009).
- [13] L. Perfetti *et al.*, Phys. Rev. Lett. **96**, 027401 (2006); T. Kampfrath *et al.*, Phys. Rev. Lett. **101**, 267403 (2008).
- [14] M. C. Beard, J. L. Blackburn, and M. J. Heben, Nano. Lett. **8**, 4238 (2008).
- [15] H. Zhao *et al.*, Phys. Rev. B **73**, 075403 (2006).
- [16] L. Luer *et al.*, Phys. Rev. B **80**, 205411 (2009).
- [17] The probe was spectrally resolved (10 nm resolution).
- [18] S. M. Bachilo *et al.*, J. Am. Chem. Soc. **125**, 11186 (2003).
- [19] O. N. Torrens, D. E. Milkie, M. Zheng, and J. M. Kikkawa, Nano Lett. **6**, 2864 (2006).
- [20] Differences in this splitting can arise from the dissimilar embedding matrices i.e. dielectric constants.
- [21] It appears due to a downward step at exactly the 178 meV vibrational resonance in the PE matrix.
- [22] A. Jorio *et al.*, Phys. Rev. B **72**, 075207 (2005).
- [23] H. D. Cornean, T. G. Pedersen, and B. Ricaud, Cont. Math. **447**, 45 (2007).
- [24] A. Jorio *et al.*, Phys. Rev. B **71**, 075401 (2005).
- [25] S. Berciaud, L. Cognet, and B. Lounis, Phys. Rev. Lett. **101**, 077402 (2008).
- [26] S. Schmittrink, D. S. Chemla, and D. A. B. Miller, Phys. Rev. B **32**, 6601 (1985).
- [27] B. I. Greene, J. Orenstein, R. R. Millard, and L. R. Williams, Phys. Rev. Lett. **58**, 2750 (1987).

DISCLAIMER

This document was prepared as an account of work sponsored by the United States Government. While this document is believed to contain correct information, neither the United States Government nor any agency thereof, nor The Regents of the University of California, nor any of their employees, makes any warranty, express or implied, or assumes any legal responsibility for the accuracy, completeness, or usefulness of any information, apparatus, product, or process disclosed, or represents that its use would not infringe privately owned rights. Reference herein to any specific commercial product, process, or service by its trade name, trademark, manufacturer, or otherwise, does not necessarily constitute or imply its endorsement, recommendation, or favoring by the United States Government or any agency thereof, or The Regents of the University of California. The views and opinions of authors expressed herein do not necessarily state or reflect those of the United States Government or any agency thereof or The Regents of the University of California.